THE JOURNAL OF PHYSICAL CHEMISTRY C
A JOURNAL OF THE AMERICAN CHEMICAL SOCIETY

pubs.acs.org/JPCC

Article

Mixed Metals Slow Down Nonradiative Recombination in Saddle-Shaped Porphyrin Nanorings: A Time-Domain Atomistic Simulation

Published as part of The Journal of Physical Chemistry virtual special issue "125 Years of The Journal of Physical Chemistry".

Ritabrata Sarkar, Md Habib, Sergiy M. Kovalenko, Sougata Pal,* and Oleg V. Prezhdo*

Cite This: *J. Phys. Chem. C* 2021, 125, 16620−16628

Read Online

ACCESS | Metrics & More | Article Recommendations | Supporting Information

ABSTRACT: Saddle-shaped zinc porphyrin nanorings are utilized as light-harvesting materials. To achieve high performance, both fast charge transfer and slow charge recombination are required. Fast transfer favors efficient separation of exciton into free carriers, enhancing photocurrent. Slow recombination reduces charge and energy losses. We simulated both processes using time-dependent self-consistent-charge density functional tight binding theory combined with nonadiabatic (NA) molecular dynamics. The obtained picosecond charge recombination times agree well with experiment. The simulations demonstrate that the carrier lifetime depends strongly on the metals present in the porphyrin nanoring. When the porphyrin units are composed of Zn centers only, the simulated lifetime is 55 ps. If nanorings contain both Zn and Cd, the nonradiative recombination is suppressed to 200 ps, nearly 4 times. Incorporation of Cd partially localizes the photogenerated charges, weakens the NA coupling, and accelerates phonon-induced loss of electronic coherence. The heavier and slower Cd also decreases the NA coupling. The nonradiative recombination is driven by low-frequency phonons, with a moderate contribution from the C−C stretch. Our study demonstrates a straightforward pathway to reducing charge losses in the porphyrin nanorings by partial exchange of Zn atoms with Cd and provides a valuable guideline for improvement of the material efficiency for solar energy applications.

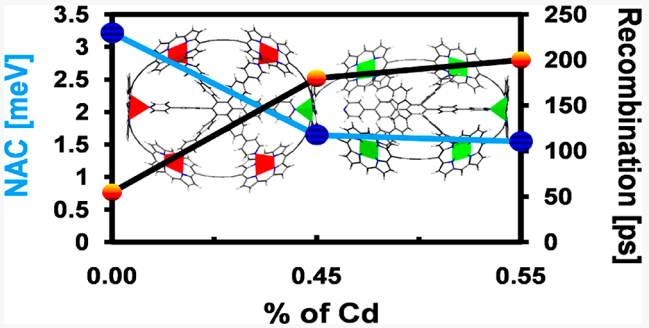

1. INTRODUCTION

Metal-centered porphyrin is the key element of the chlorophyll pigment in green plants. Porphyrins absorbed photons from solar radiation and store the photon energy as chemical energy by multistep photoinduced electron transfer processes. In past decades, macromolecular porphyrin architectures attracted immense interest in the scientific community because of their potential application as artificial photosynthetic light-harvesting materials,[1−3] chemical sensors,[4−6] metal detectors,[7] organic light-emitting diodes,[8] molecular switches,[9] memories,[10] and molecular photocatalysts.[11,12] Porphyrin nanorings, fully π-conjugated systems, possess large absorption coefficients,[13,14] extended charge state lifetimes,[15] high charge carrier mobility,[16−18] and flexible optical gap modulation by different chemical environments.[19−21] Combined with ultrafast delocalization of the electronic excitation,[13,14,22] these propertied make the nanoring systems excellent components for next-generation solar cells.

Photoexcitation of a light absorber promotes charge transfer from donor to acceptor, the primary criterion of photovoltaic materials. Charge recombination is another fundamental physical process by which charges annihilate by decay to the ground state. Recombination of photogenerated charges plays a vital role in governing the efficiency of optoelectronic devices because it reduces charge collection,[23] exciton density,[24] and open-circuit voltage.[25] The loss of photogenerated carriers by nonradiative recombination should be minimized. The rate of charge recombination should be sufficiently slow to allow charge diffusion and collection. To this end, a variety of approaches have been adopted, mainly from a molecular engineering standpoint. As evident from previous reports, the rate of nonradiative charge recombination increases due to various factors such as low semiconductor band gap,[26] large nonadiabatic (NA) coupling between the band edge states,[27] high density of trap states due to defects[28,29] or doping,[30] and the presence of conical intersections between potential energy surfaces.[31] Size[32,33] and shape[34] of semiconducting nanoma-

Received: May 30, 2021
Revised: July 7, 2021
Published: July 22, 2021

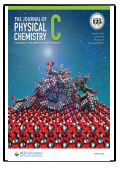

https://doi.org/10.1021/acs.jpcc.1c04749
J. Phys. Chem. C 2021, 125, 16620−16628

terials also control charge relaxation dynamics. The interaction type, for example, covalent vs noncovalent, between donor and acceptor influences the carrier recombination dynamics as well.[35] Physical parameters, such as temperature,[34,36] pressure,[37,38] and dielectric environment,[39] also affect the recombination process. The impact of quantum confinement on the charge separation and recombination processes has been investigated very recently by Musaev et al., who demonstrated an exponential decrease in both processes with increasing system size.[40]

Saddle-shaped zinc porphyrin nanorings possessing a unique geometry have been synthesized by Anderson and his group.[13] Their investigation reveals that ultrafast intramolecular charge transfer takes place between the two orthogonal rings. Such observation renders porphyrin nanorings a suitable component for photovoltaic applications. Still, the charge recombination dynamics in these systems remains unexplored. Because carrier lifetime is a key characteristic of optoelectronic devices, it is therefore essential to explore the electron−hole (e−h) recombination mechanism by assessing the dynamical behavior of charge carriers.

In this work, motivated by the experiments,[13] we have studied the e−h separation and recombination dynamics in unique saddle-shaped porphyrin nanorings. By nonadiabatic molecular dynamics (NAMD) simulation, we demonstrate that the carrier lifetime depends strongly on the metals present in the nanoring. When the nanoring is composed of 11 zinc (Zn) porphyrin units, the simulated lifetime is 55 ps. If five units contain cadmium (Cd), the charges recombine considerably slower, 180 ps. Introduction of six Cd centers suppressed the nonradiative e−h recombination further to 200 ps. The simulations show that charge localization, the NA coupling strength, phonon-induced quantum coherence loss, and participation of particular vibrations are the leading factors that govern the carrier dynamics. All these factors collectively extend the lifetime of the photogenerated carriers in the heterometal nanorings. Introduction of Cd ceases partial localization of the electron, decreasing its overlap with the hole and leading to a weaker NA coupling. The heavier and slower Cd also contributes to the NA coupling decrease. The increased localization and decreased overlap of electron and hole result in a faster coherence loss, delaying charge recombination. The simulations show that the nonradiative decay is induced primarily by low-frequency modes, with a minor contribution of C−C stretches. The reported simulations establish the mechanism of the charge carrier losses and demonstrate how the losses can be reduced by the porphyrin design strategy.

2. METHODS

The e−h recombination dynamics of the porphyrin nanoring systems are modeled with a mixed quantum-classical approach[41] combining NAMD with self-consistent-charge density functional tight binding (SCC-DFTB)[42] methodology. SCC-DFTB is a very efficient method for treating systems having a large number of atoms that otherwise cannot be treated by ab initio DFT. The electrons are treated quantum mechanically, and the nuclear degrees of freedom are treated with classical Newton's equation of motion with a semiclassical correction for decoherence. The classical path approximation (CPA)[43,44] is employed in the NAMD simulation. CPA is applicable when any significant structural changes such as isomerization, reorganization, or fragmentation do not occur due to an electronic transition, and the nuclear dynamics is dominated by thermal fluctuations. To account for the effect of decoherence, the decoherence-induced surface hopping (DISH)[45] approach is used, as implemented in the PYthon eXtension for Ab Initio Dynamics (PYXAID) code.[46,47] The SCC-DFTB method combined with NAMD has been successfully employed in a variety of systems including CNT nanohybrid composites,[48−52] cadmium chalcogenide quantum dots[53] and nanoplatelets,[54,55] and porphyrin macromolecular systems.[56] The closely related approach based on ab initio DFT has been applied to an even broader set of systems.[57−65] The details of the theoretical method are given in the Supporting Information.

All the quantum-mechanical calculations, along with geometry optimization and MD, are performed with the SCC-DFTB methodology for all the porphyrin nanoring systems. For C, H, and N, we have used the mio parameter set,[42] and for the metal atoms we used our own parameter set,[66,67] which is compatible with the mio set. After optimization of the geometry at 0 K, all nanoring systems are heated to 300 K for 5 ps with velocity rescaling.[68] Then 3 ps adiabatic MD trajectories with the atomic time step of 1 fs are generated by using the Verlet algorithm.[69] Using these 3000 configurations of each femtosecond for all the systems, we have calculated the energy of each configuration and time-dependent NA coupling values between the states involved in the carrier dynamics under investigation. Time-dependent energy and NA coupling matrices are used to perform the NAMD simulations for the charge separation and recombination dynamics in the porphyrin nanoring systems.

3. RESULTS AND DISCUSSION

3.1. Geometric and Electronic Structure. A schematic of the energy levels involved in the photoinduced charge carrier dynamics in the porphyrin nanorings is displayed in Figure 1a. Interaction of photon with a nanoring generates excitons across the band gap. The photoexcitation is followed by intramolecular charge transfer between the orthogonal

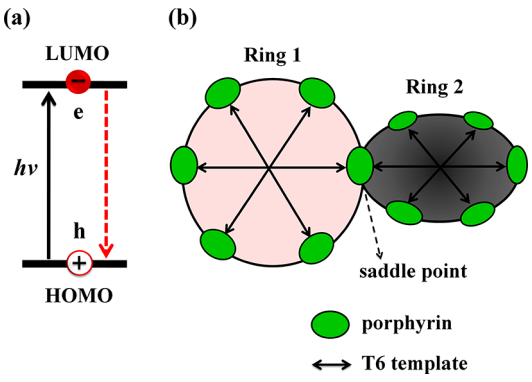

Figure 1. Schematic of the energy levels involved in the photoinduced charge carrier dynamics in the porphyrin nanoring. Photon absorption promotes an electron to the LUMO, leaving a hole in the HOMO. These charge carriers can recombine nonradiatively, as shown by the red dashed line (a). Cartoon representation of a typical saddle-shaped porphyrin nanoring, in which two porphyrin rings are orthogonal through a central porphyrin unit (b). The green ovals denote the porphyrin unit present in the nanoring. The hexadentate template T6 that binds each ring through an N atom is indicated by the double-sided arrow.

https://doi.org/10.1021/acs.jpcc.1c04749
J. Phys. Chem. C 2021, 125, 16620−16628

rings. The photogenerated carriers can undergo recombination, and the systems relax to the ground state. First, we focus on the geometric and electronic structure of porphyrin nanorings, since knowledge of the geometry and electronic properties of a system constitutes a key step for analysis of the photoinduced carrier dynamics. Second, the electron−phonon interactions that drive the photoinduced carrier relaxation dynamics are discussed in detail.

A schematic representation of the saddle-shaped porphyrin nanoring is shown in Figure 1b. Each porphyrin ring is constructed by six zinc porphyrin units connected with acetylenic linker chains. A hexadentate template firmly coordinates the central atom of the porphyrin internally as "spokes in a tire". Two porphyrin rings (Ring 1 and Ring 2) are perpendicularly meso-fused through a porphyrin unit. The junction porphyrin is the common portion of both rings.

The optimized geometry of the 11 Zn-centered porphyrin nanoring Zn[Zn]Zn is presented in Figure 2a. The first "Zn" is

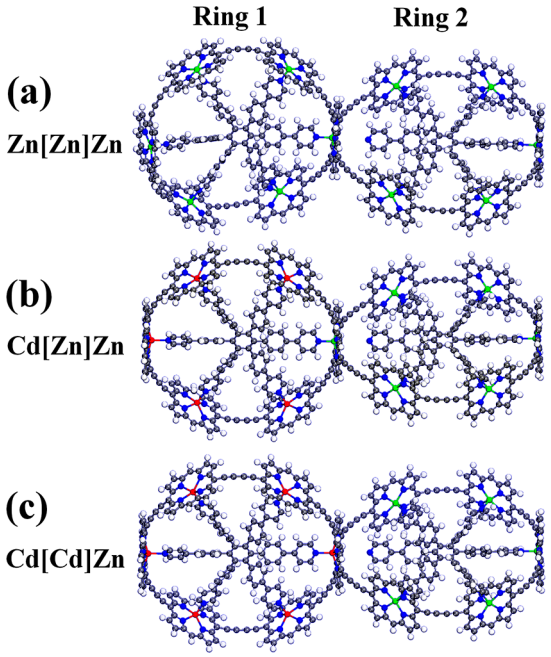

Figure 2. Ground state optimized structures of the saddle-shaped porphyrin nanorings. In Zn[Zn]Zn, 11 porphyrin units are Zn-centered (a). This nanoring is spiro-fused with perpendicular orientation of the two rings (Ring 1 and Ring 2). All porphyrin units in the nanoring are coordinated by two T6 templates. In heterometal Cd[Zn]Zn, the five Zn centers of Ring 1 are substituted with Cd (b). In Cd[Cd]Zn, another Cd is introduced into the central porphyrin unit (c), such that the Cd[Cd]Zn system contains six Cd centers along with five Zn centers. Carbon, hydrogen, nitrogen, zinc, and cadmium atoms are denoted by dark gray, white, blue, green, and red spheres, respectively.

the short notation of Ring 1, in which a hexadentate hexapyridyl (T6) template coordinates each Zn through the N atom. The second "[Zn]" term indicates the central porphyrin unit, common to both orthogonal rings, whereas the last "Zn" term denotes Ring 2. The beauty of this macrostructure is that each Zn atom is pentacoordinated except for the junction porphyrin central metal atom. The calculated Zn−N distance between the central porphyrin's Zn to N of T6 in Ring 1 is 2.1 Å. The corresponding Zn−N distance between the central porphyrin Zn to N of T6 in Ring 2 is longer, 4.6 Å. This implies that Zn of the central porphyrin unit is pseudo-hexacoordinated, in agreement with the experiment.[13] The bond strengths between the two templates and the metal of the common porphyrin are not the same; one is much stronger than the other. This asymmetry makes the intramolecular charge transfer feasible between two rings.

Along with the homometal Zn[Zn]Zn ring, two heterometal nanorings with partial substitution of Zn by Cd are also modeled to unravel the role of metal in the photoinduced excited state carrier dynamics. In heterometal Cd[Zn]Zn, the five Zn centers of Ring 1 are substituted with Cd (Figure 2b). In Cd[Zn]Zn, the Zn−N bond between the central porphyrin Zn to N of T6 in Ring 1 is 2.09 Å long. The corresponding Zn−N distance between the central porphyrin Zn to N of T6 in Ring 1 is longer, 5.1 Å. This implies that Zn of the central porphyrin unit is pseudo-hexacoordinated. In Cd[Cd]Zn, we further introduce a Cd into the central porphyrin unit (Figure 2c). Hence, the Cd[Cd]Zn system contains six Cd atoms along with five Zn atoms. The geometry of the porphyrin nanorings remains unaffected with the metal substitution even though they are molecular systems because the porphyrin rings are firmly held by the template structure. All the nanorings possess structural asymmetry in the template and common porphyrin junction. Randomly selected geometries from the 3 ps MD trajectory at 300 K have similar structural characteristics but exhibit some deformation because of thermal fluctuations (see Figure S1).

Figure 3 presents the projected density of states (PDOS) for all systems under investigation. The PDOS is separated into the contribution of Ring 1, Ring 2, and Common components. Each system possesses quasi-type-II band alignment. Photoexcitation of the nanoring promotes an electron from its highest occupied molecular orbital (HOMO) to its lowest unoccupied molecular orbital (LUMO), thereby generating an e−h pair. The HOMO wave function is entirely delocalized over the whole nanoring for each system. In contrast, the LUMO is localized over Ring 1 only. Localization of electronic charge of the final and initial states is confirmed by the distribution of charge density of each system (Figure S2). There is no notable change in the charge densities of homo- and heterometal porphyrin nanorings observed. But the different localization of charge of the states involved in the e−h recombination, that is, the HOMO comes from porphyrin rings and T6 contributed to the LUMO, reduces the spatial overlap between them and slows the recombination processes. The exciton in the charge-separated state is formed by the electron localized on the inner part of a ring, and the hole localized primarily on the central region connecting the two rings, with contributions from the outer parts of the rings (Figure S2). There is very little overlap between the HOMO and the LUMO, indicating that it is a charge-separated state. For the Zn[Zn]Zn nanoring, the simulated energy gap is 0.59 eV. Introduction of Cd centers into the nanorings causes gap contraction (Figure 3b,c and Table 1). The decrease in the optical gap is explained by the increasing molecular weight of the macrostructures with the replacement of Zn by Cd; this is similar to our previous work.[56]

The nonradiative quantum transition is governed by NA coupling present between the initial and final states. The NA coupling between two adiabatic states i and j is expressed as $d_{ij} = \left\langle \phi_i(r, R(t)) \middle| \frac{\partial \phi_j(r, R(t))}{\partial t} \right\rangle$. The strength of the coupling

https://doi.org/10.1021/acs.jpcc.1c04749
J. Phys. Chem. C 2021, 125, 16620−16628

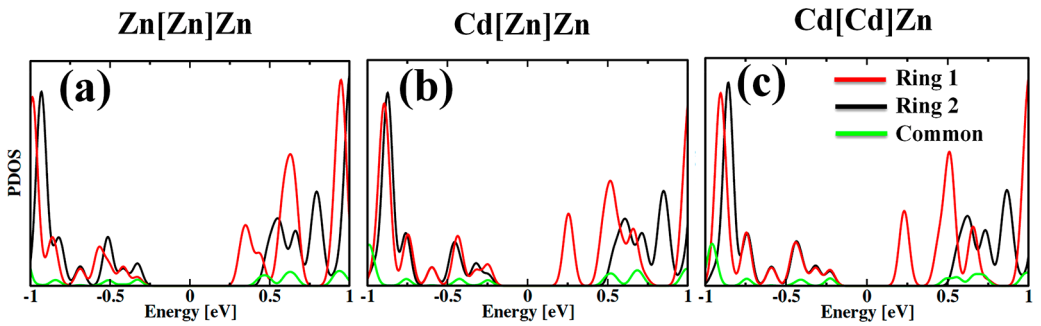

Figure 3. Projected density of states (PDOS) of the optimized structures of Zn[Zn]Zn (a), Cd[Zn]Zn (b), and Cd[Cd]Zn (c). PDOS is split into contributions of Ring 1, Ring 2, and Common components. The Fermi energy is set to be zero. Each system possesses quasi-type-II band alignment, with electron localized on Ring 1 (LUMO) and hole delocalized on the entire nanoring (HOMO).

Table 1. Canonically Averaged Energy Gap, Root-Mean-Square (rms) Nonadiabatic (NA) Coupling, Decoherence Time, and e−h Recombination Time Scales for the Porphyrin Nanoring Systems

system	av energy gap (eV)	rms NA coupling (meV)	decoherence (fs)	time (ps)
Zn[Zn]Zn	0.59	3.22	14	55
Cd[Zn]Zn	0.48	1.65	9	180
Cd[Cd]Zn	0.43	1.55	9	200

depends on the overlap of the wave functions between the pair of states which is parametrically depending on the nuclear coordinates (R). The simulated NA coupling between the HOMO and LUMO states of Zn[Zn]Zn is 3.22 meV (Table 1). One can observe weaker NA electron−phonon coupling for both heterometal rings. The NA coupling is reduced to half (1.65 meV) for the Cd[Zn]Zn nanoring. Further weakening of the coupling strength (1.55 meV) is observed for Cd[Cd]Zn. Generally, the NA coupling is inversely proportional to the energy gap. Interestingly, the NA coupling decreases when the energy gap decreases in the current systems (Table 1). This is unusual and can be explained by two other arguments. In addition to the energy gap dependence, the NA coupling is proportional to the atomic velocity, which in turn depends on atomic mass. Because Cd is heavier than Zn, it leads to a smaller NA coupling. The NA coupling also depends on the nuclear gradient matrix element between the initial and final electronic wave function. Introduction of Cd breaks the symmetry of the system that contains only Zn. This leads to partial localization of the initial and final wave functions and hence to a decreased matrix element. Considering the metal-dependent NA coupling between the states, the nonradiative e−h recombination should be slower in the heterometal nanorings compared to the homometal system. Substitution of Cd in the central porphyrin unit has a strong influence on the e−h recombination dynamics. The e−h recombination dynamics depends on the NA electronic−vibrational coupling present between the excited and ground states. The electronic−vibrational coupling also determines fluctuations of the energies of the two states. The PDOS in Figure 3 and the charge densities in Figure S2 demonstrate that the HOMO has a strong contribution from the central porphyrin unit. Substitution of Zn with the heavier Cd in the central porphyrin slows vibrational motions and decreases the NA coupling. In addition, when the central unit is a Zn porphyrin, one of the porphyrin rings is fully Zn-metallized and the other is partially Cd-metallized. Replacing Zn by Cd in the central unit reverses this situation. Our study demonstrates the effect of partial vs entire Cd substitution of a porphyrin ring of the nanoring system on the recombination dynamics. In particular, the partially Cd-substituted system has faster recombination compared to the fully Cd-substituted ring.

3.2. Electronic−Vibrational Interactions. The electron−phonon interactions are responsible for two related but different phenomenon, that is, inelastic and elastic processes. The former process leads to energy exchange between the electronic and vibrational subsystem. The electronic energy generated upon photoexcitation is lost to heat and thereby

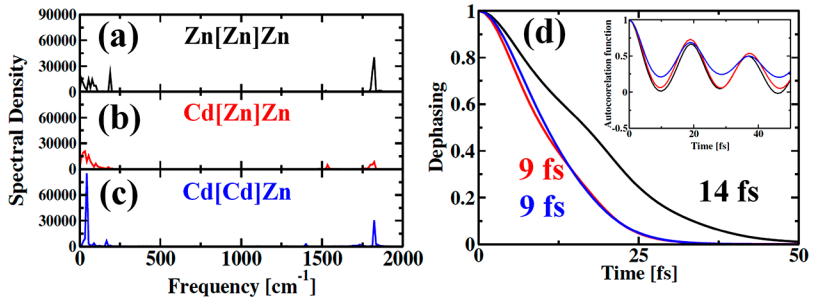

Figure 4. Fourier transformations (FTs) of fluctuations of the energy gap between HOMO and LUMO in Zn[Zn]Zn (a), Cd[Zn]Zn (b), and Cd[Cd]Zn (c). Both low- and high-frequency modes are involved during the carrier recombination for all systems. In the heterometal nanorings low-frequency vibrations become more prominent. Pure dephasing functions for the lowest energy photoexcitation in Zn[Zn]Zn (black line), Cd[Zn]Zn (red line), and Cd[Cd]Zn (blue line) at room temperature (d). Simulated data are fitted with a Gaussian function. The phonon-induced loss of electronic coherence is faster in the heterometal nanorings, favoring slower carrier relaxation. The autocorrelation functions (ACFs) are shown in the inset. The color code for the dephasing curves and ACFs is the same as for the FTs.

https://doi.org/10.1021/acs.jpcc.1c04749
J. Phys. Chem. C 2021, 125, 16620−16628

decreases the voltage of a solar device. The rate of nonradiative e−h recombination depends on the participation of phonon modes because they are coupled with the electronic subsystem and facilitate phonon energy dispersion during the e−h recombination process. We compute spectral densities by applying the Fourier transforms (FTs) of fluctuations of the pair of states within fundamental energy gaps of the nanoring systems. The spectral density of FTs is also known as influence spectra are presented in Figure 4. The intensity of each peak in the influence spectrum characterizes the strength of electron−phonon coupling at a particular vibrational frequency.[51,70] Both low (<250 cm^{-1}) and high (1500−2000 cm^{-1}) frequency modes are involved in e−h recombination for all the systems. The modes below the 250 cm^{-1} are mainly evolved from out-of-plane vibration of porphyrin units. In turn, the higher frequency mode around 1800 cm^{-1} is assigned due to the in-plane vibration of porphyrin units in the ring.[71] In the case of Zn[Zn]Zn, a strong peak near 1800 cm^{-1} frequency along with a broad range of low-frequency modes is mainly contributed to charge carrier relaxation (Figure 4a). This dominant high-frequency out-of-plane vibration contributes strongly to the charge phonon coupling because their motion is fast and creates large nuclear velocity that enters into the NA coupling matrix element. This observation is consistent with stronger NA charge phonon coupling with a magnitude of 3.22 meV (Table 1). The spectral density of the Cd[Zn]Zn nanoring is notably distinct from the Zn[Zn]Zn ring (Figure 4b). Note that mainly low-frequency phonons with higher phonon peaks participate in the carrier recombination. It is worth mentioning that such peak intensities are low as compared to Zn[Zn]Zn. Not only the position of phonon peaks in the spectral density but also the heights of the peaks are also a major point of concern. As stated, the strength of the electron−phonon coupling is proportional to the heights of the peaks. Thus, the resulting NA coupling is affected and shows weak coupling strength, 1.65 meV. This is manifested due to a lower nuclear motion of the heavier Cd atoms in the ring. The system with Cd[Cd]Zn exhibits both high- and low-frequency vibrational modes for charge recombination (Figure 4c). The low-frequency mode at 50 cm^{-1} predominantly creates a smaller NA coupling of 1.55 meV. This correlated to the larger height of this peak compared to the peak at 1800 cm^{-1} of the influence spectrum. In the presence of Cd, the porphyrin units and the template form stronger bonding compared to the Zn system. Because of the stronger bindings, the in-plane vibrations of the porphyrin units are modified. In particular, the Cd substitutions in the nanoring system activate more lower frequency modes, which dominate over the higher range modes (Figure 4) because high-frequency modes arise from in-plane vibrations of the porphyrin units. On the basis of the analysis of spectral density followed by NA coupling between the pair of states, we expect that the carrier relaxation would be slower for the heterometal systems.

The elastic electronic−vibrational interaction randomizes the phases (momenta) of electronic wave functions, which causes the loss of quantum coherence between the pair of HOMO and LUMO states. We simulate the decoherence time as pure dephasing time based on optical response theory[72] with the second-order cumulant approximation. The time scales are obtained from the Gaussian function fitting $y = A \exp(-0.5[t/\tau_{gau}]^2)$ of the simulated data in Figure 4d, where τ_{gau} is the decoherence time constant. The decoherence times are presented in Table 1. Nonradiative e−h recombination times of the three systems under study are significantly larger than the sub-15 fs pure decoherence times. Thus, the decoherence effect in the present NAMD simulation is included. The simulated decoherence time for Zn[Zn]Zn is 14 fs. In contrast, for heterometal systems, the pair of HOMO and LUMO states remains in coherence for 9 fs. The phonon-induced loss of electronic coherence is rapid for the heterometal nanoring. Note that shorter electronic coherence delays the quantum transition due to the quantum Zeno effect.[73,74] Thus, the rate of e−h recombination is slower in the heterometal nanoring compared to Zn[Zn]Zn. Autocorrelation functions (ACFs) of HOMO−LUMO energy gap fluctuations of all systems are shown in the inset of Figure 4d. All the ACFs have started with the initial value of 1 because our calculated ACFs are normalized. ACFs characterize the memory of the energy gap fluctuation. The sequence of ACF decays for the porphyrin nanoring systems is Zn[Zn]Zn > Cd[Zn]Zn > Cd[Cd]Zn, losing the phase information as well. The slower decay of ACFs is characterized by the rapid decoherence between the electronic states in the heterometal nanoring.

3.3. Charge Transfer Dynamics. Figure 5 presents the evolution of the population of the donor states for photo-induced charge transfer in the nanoring systems under investigation. Fitting the data using a linear combination of the Gaussian and exponential function $y = A \exp(-t/\tau_{exp}) + (1 - A) \exp[t/\tau_{gau}]^2$ gives the characteristic time scales as reported in the figure. The simulated intramolecular charge transfer time in the Zn[Zn]Zn is 55 fs. The population transition is ultrafast, and this observation agrees well with the experiment.[13] It should be mentioned that such an intramolecular charge transition rate is also similar to that taking place on sub-50 fs for heterometal systems. It indicates that the charge transfer is not influenced by the Cd incorporation into the ring, but heterometal systems ensure ultrafast charge transfer. The analysis of the observed charge transfer dynamics can be found in the Supporting Information. It is important to emphasize that not only the rapid charge separation dynamics but also slow charge carrier relaxation is important to achieve high efficiencies, in particular, by reducing charge losses. Keeping this in mind, the subsequent section deals with the nonradiative carrier recombination dynamics. Special attention is paid to the role of Cd incorporation into the ring.

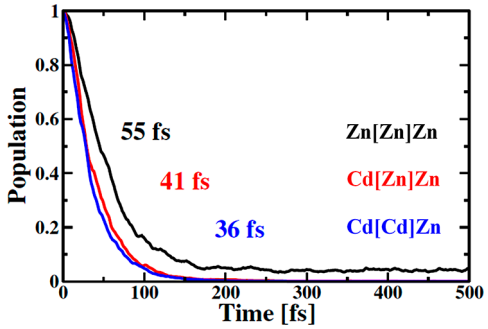

Figure 5. Decay of population of the donor state during the charge transfer dynamics in Zn[Zn]Zn (black line), Cd[Zn]Zn (red line), and Cd[Cd]Zn (blue line). The time scales are obtained from fits to linear combination of Gaussian and exponential functions. Photoexcitation of Zn[Zn]Zn leads to intramolecular ultrafast charge transfer, well matched with experiment. The incorporation of Cd into the nanoring does not significantly change the charge separation time.

https://doi.org/10.1021/acs.jpcc.1c04749
J. Phys. Chem. C 2021, 125, 16620−16628

3.4. Nonradiative e−h Recombination. The nonradiative excited carrier recombination constitutes the major mechanism for charge and energy losses in a solar cell device. Therefore, a topmost priority is to ensure slow carrier recombination to achieve effective device performance. The evolution of population of the excited states of 5 ps time period during the nonradiative charge recombination in the porphyrin nanorings is represented in Figure 6a. The stimulated data are

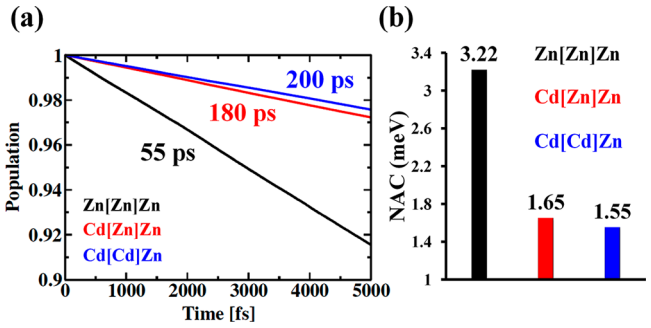

Figure 6. Population decay due to nonradiative e−h recombination in Zn[Zn]Zn, Cd[Zn]Zn, and Cd[Cd]Zn (a). The relaxation dynamics is performed by DISH. The time scales are obtained from short time linear approximation to exponential decay. The lifetime of the photogenerated charge is strongly dependent on the metals present in the nanoring. In Cd[Cd]Zn, the carrier relaxation is suppressed by a factor of 4 with a time constant of 200 ps. Root-mean square value of NA coupling for e−h recombination in the nanoring systems under study (b). Weaker NA coupling, faster pure dephasing, and participation of low-frequency phonon modes suppress charge recombination in heterometal systems.

obtained from NAMD simulation and fitted with short-time linear approximation to the exponential function $y = A\exp(-t/\tau)$, where τ is the time constant for e−h recombination. The obtained time scales are in the picosecond time regime, which is well corroborated with both theory[48,56] and experiment.[75,76] The photogenerated carriers recombine within 55 ps between the frontier orbitals of Zn[Zn]Zn (Figure 6a and Table 1). The influence of Cd insertion into the nanoring on the excited state lifetime is much more significant compared to intramolecular charge transfer dynamics. The rate of e−h recombination for Cd[Zn]Zn is significantly suppressed by a factor of about more than 3, with a time constant of 180 ps. An even longer lifetime (200 ps) is achieved for the Cd[Cd]Zn nanoring. The present investigation revealed that longer-lived charge carrier can be achieved by judicious incorporation of Cd atom in the nanoring.

Several factors rationalize these observations, such as (1) NA coupling strength, (2) nature of phonon modes, and (3) quantum coherence between the pair of concerned electronic states. The most important factor is NA coupling, which shows a collective effect of electronic−vibrational interactions that govern the fate of the photogenerated carrier dynamics. As evident from Figure 6b and Table 1, the stronger NA coupling (3.22 meV) induces rapid charge recombination (55 ps) in Zn[Zn]Zn. The simulated NA charge phonon strength is greatly reduced to a factor 2 (1.65 meV) for the Cd[Zn]Zn nanoring compared to the Zn[Zn]Zn nanoring. Furthermore, significant weakening of the coupling strength (1.55 meV) is observed too for Cd[Cd]Zn. We argued that the rate of NA charge recombination is mostly guided by the strength of NA charge phonon interaction between the pair of HOMO−LUMO wave functions. As evident from Table 1, the band gap decreases with the introduction of heavier Cd centers into the nanoring. Therefore, one might expect faster charge carrier relaxation in heterometal systems. But weak NA charge phonon coupling competes with the low band gap and drives the quantum transition at a slower rate. Thus, with an increase of Cd center, the decay of exciton is greatly suppressed and thereby minimizes the charge losses. The NA e−h relaxation in Zn[Zn]Zn is also governed by the participation of both low- and dominant high-frequency vibration (Figure 4a). Hence, it experiences rapid charge carrier relaxation to the ground state. For heterometal ring the carrier relaxes through intense low-frequency out-of-plane vibration (Figure 4b,c). Such low-frequency modes couple with the electronic subsystem participating in the relaxation process and contribute to a longer carrier lifetime. Moreover, the quantum coherence is of longer-lived (14 fs) for Zn[Zn]Zn (Table 1 and Figure 4d). When Cd is introduced into the ring, the heterometal system experiences shorter electronic coherence (9 fs). Thus, phonon-induced coherence significantly slows the quantum transition and hence decelerated the charge losses to heat. Also, faster decay of ACFs of Zn[Zn]Zn causes strong electronic coherence between the states involved in e−h recombination. In heterometal systems, the lifetime increases with the higher molecular weights, agreeing well with the earlier findings.[77,78]

The nonradiative charge recombination depends on three factors in our simulations. These are the energy gap, the NA coupling, and the decoherence time. Typically, a larger energy gap, a smaller NA coupling, and a shorter coherence time lead to a slower nonradiative transition. The NA coupling and the decoherence times are the two factors that rationalize the changes in the recombination time, while the energy gap acts to counteract the trend (Table 1). The NA coupling and the decoherence time depend on atomic motions and on overlap of electron and hole densities. The heavier Cd atoms have smaller velocities and lead to smaller NA coupling and slower coherence loss. Introduction of Cd into the Zn-based systems partially localizes electron and hole, leading to smaller NA coupling and faster decoherence. The data show that the systems with Cd exhibit smaller NA coupling and faster decoherence. Therefore, localization of the electron and hole is the most important factor, since only the localization can explain the changes in both the NA coupling and the coherence time. On the basis of this conclusion, one can expect that a complete replacement of Zn with Cd will restore delocalization of electron and hole and shorten the lifetime of the charge-separated state. The present simulation demonstrates that long-lived charge carriers can be obtained by judicious incorporation of Cd centers into the homometal Zn nanoring, reducing energy and charge losses and improving the photovoltaic efficiency.

4. CONCLUSIONS

In summary, the nonradiative excited state dynamics of both homo- and heterometal porphyrin nanorings are extensively studied by applying the SCC-DFTB method combined with the NAMD methodology. The simulation confirms the ultrafast intramolecular charge separation in Zn[Zn]Zn as reported in the recent experiments. The charge transfer time changes little upon incorporation of five or six Cd centers in the nanoring. On the other hand, we demonstrate that the photogenerated charge carrier lifetime depends strongly on the metal present in the saddle-shaped porphyrin nanoring. The

https://doi.org/10.1021/acs.jpcc.1c04749
J. Phys. Chem. C 2021, 125, 16620−16628

simulated e−h recombination time is 55 ps for the Zn[Zn]Zn nanoring. The lifetime increases by a factor of 3 to 180 ps with the incorporation of five Cd centers into the nanoring. When six Cd centers are introduced, the e−h recombination is suppressed further by almost a factor of 4 relative to Zn[Zn]Zn, with a time constant of 200 ps. Analysis of the simulations reveals that the NA coupling strength, the time of phonon-induced quantum decoherence, and active vibrations are the leading factors that govern the carrier dynamics. The presence of multiple metals localizes partially the electron wave function, reduces e−h overlap, decreases the NA coupling, and accelerates coherence loss. The slower motions of the heavier Cd atoms further contribute to the NA coupling reduction. The photoinduced charge separation is driven strongly by the faster C−C stretching motions, while the e−h recombination occurs by coupling to low-frequency modes with minor contributions from C−C stretches. Providing a detailed analysis of the charge separation and recombination mechanisms, our study demonstrates that e−h recombination can be suppressed by use of heterometal porphyrin structures, providing a valuable guideline for efficient porphyrin-based solar energy applications.

■ ASSOCIATED CONTENT

Supporting Information

The Supporting Information is available free of charge at https://pubs.acs.org/doi/10.1021/acs.jpcc.1c04749.

Details of the theoretical methodology, optimized geometry and projected density of states of the cadmium nanoring, structural conformations of the nanorings at room temperature along with electronic charge densities of the key states (PDF)

■ AUTHOR INFORMATION

Corresponding Authors

Sougata Pal − *Department of Chemistry, University of Gour Banga, Malda 732103, India;* orcid.org/0000-0002-1514-2728; Email: sougatapal_1979@yahoo.co.in

Oleg V. Prezhdo − *Department of Chemistry, University of Southern California, Los Angeles, California 90089, United States;* orcid.org/0000-0002-5140-7500; Email: prezhdo@usc.edu

Authors

Ritabrata Sarkar − *Department of Chemistry, University of Gour Banga, Malda 732103, India;* orcid.org/0000-0001-7798-1140

Md Habib − *Department of Chemistry, University of Gour Banga, Malda 732103, India; Department of Chemistry, Sripat Singh College, Jiaganj 742122, India;* orcid.org/0000-0002-7676-2293

Sergiy M. Kovalenko − *Department of Organic Chemistry, V.N. Karazin Kharkiv National University, Kharkiv 61022, Ukraine; I.M. Sechenov First Moscow State Medical University of the Ministry of Health of the Russian Federation (Sechenov University), Moscow 119991, Russian Federation*

Complete contact information is available at: https://pubs.acs.org/10.1021/acs.jpcc.1c04749

Notes

The authors declare no competing financial interest.

■ ACKNOWLEDGMENTS

R.S. is grateful to CSIR for his Senior Research Fellowship. S.P. acknowledges the financial support from CSIR (01(2956)/18/EMR-II), Govt. of India. O.V.P. acknowledges funding from the US National Science Foundation (Grant CHE-1900510).

■ REFERENCES

(1) Pruchyathamkorn, J.; Kendrick, W. J.; Frawley, A. T.; Mattioni, A.; Caycedo-Soler, F.; Huelga, S. F.; Plenio, M. B.; Anderson, H. L. A Complex Comprising a Cyanine Dye Rotaxane and a Porphyrin Nanoring as a Model Light-Harvesting System. *Angew. Chem., Int. Ed.* **2020**, *59*, 16455−16458.

(2) Li, L.-L.; Diau, E. W.-G. Porphyrin-Sensitized Solar Cells. *Chem. Soc. Rev.* **2013**, *42*, 291−304.

(3) Kundu, S.; Patra, A. Nanoscale Strategies for Light Harvesting. *Chem. Rev.* **2017**, *117*, 712−757.

(4) Papkovsky, D. B.; Ponomarev, G. V.; Trettnak, W.; O'Leary, P. Phosphorescent Complexes of Porphyrin Ketones: Optical Properties and Application to Oxygen Sensing. *Anal. Chem.* **1995**, *67*, 4112−4117.

(5) Lvova, L.; Paolesse, R.; Di Natale, C.; D'Amico, A. Detection of Alcohols in Beverages: An Application of Porphyrin-Based Electronic Tongue. *Sens. Actuators, B* **2006**, *118*, 439−447.

(6) Paolesse, R.; Nardis, S.; Monti, D.; Stefanelli, M.; Di Natale, C. Porphyrinoids for Chemical Sensor Applications. *Chem. Rev.* **2017**, *117*, 2517−2583.

(7) Xu, Y.; Zhao, L.; Bai, H.; Hong, W.; Li, C.; Shi, G. Chemically Converted Graphene Induced Molecular Flattening of 5, 10, 15, 20-Tetrakis (1-Methyl-4-Pyridinio) Porphyrin and Its Application for Optical Detection of Cadmium (Ii) Ions. *J. Am. Chem. Soc.* **2009**, *131*, 13490−13497.

(8) Lee, S. Y.; Yasuda, T.; Komiyama, H.; Lee, J.; Adachi, C. Thermally Activated Delayed Fluorescence Polymers for Efficient Solution-Processed Organic Light-Emitting Diodes. *Adv. Mater.* **2016**, *28*, 4019−4024.

(9) Liddell, P. A.; Kodis, G.; Moore, A. L.; Moore, T. A.; Gust, D. Photonic Switching of Photoinduced Electron Transfer in a Dithienylethene− Porphyrin− Fullerene Triad Molecule. *J. Am. Chem. Soc.* **2002**, *124*, 7668−7669.

(10) Gryko, D. T.; Clausen, C.; Roth, K. M.; Dontha, N.; Bocian, D. F.; Kuhr, W. G.; Lindsey, J. S. Synthesis of "Porphyrin-Linker-Thiol" Molecules with Diverse Linkers for Studies of Molecular-Based Information Storage. *J. Org. Chem.* **2000**, *65*, 7345−7355.

(11) Imaoka, T.; Tanaka, R.; Arimoto, S.; Sakai, M.; Fujii, M.; Yamamoto, K. Probing Stepwise Complexation in Phenylazomethine Dendrimers by a Metallo-Porphyrin Core. *J. Am. Chem. Soc.* **2005**, *127*, 13896−13905.

(12) Elouarzaki, K.; Le Goff, A.; Holzinger, M.; Thery, J.; Cosnier, S. Electrocatalytic Oxidation of Glucose by Rhodium Porphyrin-Functionalized Mwcnt Electrodes: Application to a Fully Molecular Catalyst-Based Glucose/O2 Fuel Cell. *J. Am. Chem. Soc.* **2012**, *134*, 14078−14085.

(13) Favereau, L.; Cnossen, A.; Kelber, J. B.; Gong, J. Q.; Oetterli, R. M.; Cremers, J.; Herz, L. M.; Anderson, H. L. Six-Coordinate Zinc Porphyrins for Template-Directed Synthesis of Spiro-Fused Nanorings. *J. Am. Chem. Soc.* **2015**, *137*, 14256−14259.

(14) Cremers, J.; Haver, R.; Rickhaus, M.; Gong, J. Q.; Favereau, L.; Peeks, M. D.; Claridge, T. D.; Herz, L. M.; Anderson, H. L. Template-Directed Synthesis of a Conjugated Zinc Porphyrin Nanoball. *J. Am. Chem. Soc.* **2018**, *140*, 5352−5355.

(15) Leary, E.; Kastlunger, G.; Limburg, B.; Rincon-Garcia, L.; Hurtado-Gallego, J.; Gonzalez, M. T.; Bollinger, G. R.; Agrait, N.; Higgins, S. J.; Anderson, H. L.; Stadler, R.; Nichols, R. J. Long-Lived Charged States of Single Porphyrin-Tape Junctions under Ambient Conditions. *Nanoscale Horiz.* **2021**, *6*, 49.

(16) Choi, S.; Chae, S. H.; Shin, J.; Kim, Y.; Kim, S.-J.; Choi, D. H.; Lee, S. J. Dramatic Enhancement of Carrier Mobility Via Effective

Secondary Structural Arrangement Resulting from the Substituents in a Porphyrin Transistor. *Chem. Commun.* **2013**, *49*, 3994−3996.
(17) Ohta, K.; Tokonami, S.; Takahashi, K.; Tamura, Y.; Yamada, H.; Tominaga, K. Probing Charge Carrier Dynamics in Porphyrin-Based Organic Semiconductor Thin Films by Time-Resolved Thz Spectroscopy. *J. Phys. Chem. B* **2017**, *121*, 10157−10165.
(18) Leary, E.; Limburg, B.; Alanazy, A.; Sangtarash, S.; Grace, I.; Swada, K.; Esdaile, L. J.; Noori, M.; González, M. T.; Rubio-Bollinger, G.; et al. Bias-Driven Conductance Increase with Length in Porphyrin Tapes. *J. Am. Chem. Soc.* **2018**, *140*, 12877−12883.
(19) Aziz, A.; Ruiz-Salvador, A. R.; Hernández, N. C.; Calero, S.; Hamad, S.; Grau-Crespo, R. Porphyrin-Based Metal-Organic Frameworks for Solar Fuel Synthesis Photocatalysis: Band Gap Tuning Via Iron Substitutions. *J. Mater. Chem. A* **2017**, *5*, 11894−11904.
(20) Zhylitskaya, H.; Cybińska, J.; Chmielewski, P.; Lis, T.; Stepien, M. Bandgap Engineering in Π-Extended Pyrroles. A Modular Approach to Electron-Deficient Chromophores with Multi-Redox Activity. *J. Am. Chem. Soc.* **2016**, *138*, 11390−11398.
(21) Posligua, V.; Aziz, A.; Haver, R. e.; Peeks, M. D.; Anderson, H. L.; Grau-Crespo, R. Band Structures of Periodic Porphyrin Nanostructures. *J. Phys. Chem. C* **2018**, *122*, 23790−23798.
(22) Yong, C.-K.; Parkinson, P.; Kondratuk, D. V.; Chen, W.-H.; Stannard, A.; Summerfield, A.; Sprafke, J. K.; O'Sullivan, M. C.; Beton, P. H.; Anderson, H. L.; Herz, L. M. Ultrafast Delocalization of Excitation in Synthetic Light-Harvesting Nanorings. *Chem. Sci.* **2015**, *6*, 181−189.
(23) Li, Q.; Yang, Y.; Que, W.; Lian, T. Size-and Morphology-Dependent Auger Recombination in Cspbbr3 Perovskite Two-Dimensional Nanoplatelets and One-Dimensional Nanorods. *Nano Lett.* **2019**, *19*, 5620−5627.
(24) Baghani, E.; O'Leary, S. K.; Fedin, I.; Talapin, D. V.; Pelton, M. Auger-Limited Carrier Recombination and Relaxation in Cdse Colloidal Quantum Wells. *J. Phys. Chem. Lett.* **2015**, *6*, 1032−1036.
(25) Albrecht, S.; Janietz, S.; Schindler, W.; Frisch, J.; Kurpiers, J.; Kniepert, J.; Inal, S.; Pingel, P.; Fostiropoulos, K.; Koch, N.; Neher, D. Fluorinated Copolymer Pcpdtbt with Enhanced Open-Circuit Voltage and Reduced Recombination for Highly Efficient Polymer Solar Cells. *J. Am. Chem. Soc.* **2012**, *134*, 14932−14944.
(26) Englman, R.; Jortner, J. The Energy Gap Law for Non-Radiative Decay in Large Molecules. *J. Lumin.* **1970**, *1*, 134−142.
(27) Prezhdo, O. V.; Rossky, P. J. Evaluation of Quantum Transition Rates from Quantum-Classical Molecular Dynamics Simulations. *J. Chem. Phys.* **1997**, *107*, 5863−5878.
(28) Li, L.; Long, R.; Prezhdo, O. V. Why Chemical Vapor Deposition Grown Mos2 Samples Outperform Physical Vapor Deposition Samples: Time-Domain Ab Initio Analysis. *Nano Lett.* **2018**, *18*, 4008−4014.
(29) Wang, S.; Fang, W.-H.; Long, R. Hydrogen Passivated Silicon Grain Boundaries Greatly Reduce Charge Recombination for Improved Silicon/Perovskite Tandem Solar Cell Performance: Time Domain Ab Initio Analysis. *J. Phys. Chem. Lett.* **2019**, *10*, 2445−2452.
(30) Qiao, L.; Fang, W.-H.; Long, R. Dopant Control of Electron−Hole Recombination in Cesium−Titanium Halide Double Perovskite by Time Domain Ab Initio Simulation: Codoping Supersedes Monodoping. *J. Phys. Chem. Lett.* **2018**, *9*, 6907−6914.
(31) Shu, Y.; Fales, B. S.; Levine, B. G. Defect-Induced Conical Intersections Promote Nonradiative Recombination. *Nano Lett.* **2015**, *15*, 6247−6253.
(32) Liu, J.; Neukirch, A. J.; Prezhdo, O. V. Non-Radiative Electron−Hole Recombination in Silicon Clusters: Ab Initio Non-Adiabatic Molecular Dynamics. *J. Phys. Chem. C* **2014**, *118*, 20702−20709.
(33) Shang, Q.; Kaledin, A. L.; Li, Q.; Lian, T. Size Dependent Charge Separation and Recombination in Cspbi3 Perovskite Quantum Dots. *J. Chem. Phys.* **2019**, *151*, 074705.
(34) Nam, Y.; Li, L.; Lee, J. Y.; Prezhdo, O. V. Size and Shape Effects on Charge Recombination Dynamics of TiO_2 Nanoclusters. *J. Phys. Chem. C* **2018**, *122*, 5201−5208.
(35) Long, R.; Casanova, D.; Fang, W.-H.; Prezhdo, O. V. Donor−Acceptor Interaction Determines the Mechanism of Photoinduced Electron Injection from Graphene Quantum Dots into TiO_2: Π-Stacking Supersedes Covalent Bonding. *J. Am. Chem. Soc.* **2017**, *139*, 2619−2629.
(36) Li, W.; Vasenko, A. S.; Tang, J.; Prezhdo, O. V. Anharmonicity Extends Carrier Lifetimes in Lead Halide Perovskites at Elevated Temperatures. *J. Phys. Chem. Lett.* **2019**, *10*, 6219−6226.
(37) Zhou, X.; Li, L.; Dlott, D. D.; Prezhdo, O. V. Molecular Photophysics under Shock Compression: Ab Initio Nonadiabatic Molecular Dynamics of Rhodamine Dye. *J. Phys. Chem. C* **2018**, *122*, 13600−13607.
(38) Li, W.; Chen, Z.; Tang, J.; Prezhdo, O. V. Anti-Correlation between Band-Gap and Carrier Lifetime in Lead Halide Perovskites under Compression Rationalized by Ab Initio Quantum Dynamics. *Chem. Mater.* **2020**, *32*, 4707.
(39) Feskov, S. V.; Ionkin, V. N.; Ivanov, A. I.; Hagemann, H.; Vauthey, E. Solvent and Spectral Effects in the Ultrafast Charge Recombination Dynamics of Excited Donor− Acceptor Complexes. *J. Phys. Chem. A* **2008**, *112*, 594−601.
(40) Kaledin, A. L.; Lian, T.; Hill, C. L.; Musaev, D. G. An All-Atom Theory of Electron Transfer at Nanocrystal/Molecule Interfaces: A Hybrid Lcao/Dft Approach. *J. Phys. Chem. C* **2021**, *125*, 5116−5126.
(41) Pal, S.; Trivedi, D. J.; Akimov, A. V.; Aradi, B. l.; Frauenheim, T.; Prezhdo, O. V. Nonadiabatic Molecular Dynamics for Thousand Atom Systems: A Tight-Binding Approach toward Pyxaid. *J. Chem. Theory Comput.* **2016**, *12*, 1436−1448.
(42) Elstner, M.; Porezag, D.; Jungnickel, G.; Elsner, J.; Haugk, M.; Frauenheim, T.; Suhai, S.; Seifert, G. Self-Consistent-Charge Density-Functional Tight-Binding Method for Simulations of Complex Materials Properties. *Phys. Rev. B: Condens. Matter Mater. Phys.* **1998**, *58*, 7260.
(43) Augustin, S. D.; Rabitz, H. The Classical Path Approximation in Time-Dependent Quantum Collision Theory. *J. Chem. Phys.* **1978**, *69*, 4195−4200.
(44) Miller, W. H. Classical Path Approximation for the Boltzmann Density Matrix. *J. Chem. Phys.* **1971**, *55*, 3146−3149.
(45) Jaeger, H. M.; Fischer, S.; Prezhdo, O. V. Decoherence-Induced Surface Hopping. *J. Chem. Phys.* **2012**, *137*, 22A545.
(46) Akimov, A. V.; Prezhdo, O. V. The Pyxaid Program for Non-Adiabatic Molecular Dynamics in Condensed Matter Systems. *J. Chem. Theory Comput.* **2013**, *9*, 4959−4972.
(47) Akimov, A. V.; Prezhdo, O. V. Advanced Capabilities of the Pyxaid Program: Integration Schemes, Decoherence Effects, Multi-excitonic States, and Field-Matter Interaction. *J. Chem. Theory Comput.* **2014**, *10*, 789−804.
(48) Sarkar, R.; Habib, M.; Pal, S.; Prezhdo, O. V. Ultrafast, Asymmetric Charge Transfer and Slow Charge Recombination in Porphyrin/Cnt Composites Demonstrated by Time-Domain Atomistic Simulation. *Nanoscale* **2018**, *10*, 12683−12694.
(49) Pal, S.; Casanova, D.; Prezhdo, O. V. Effect of Aspect Ratio on Multiparticle Auger Recombination in Single-Walled Carbon Nanotubes: Time Domain Atomistic Simulation. *Nano Lett.* **2018**, *18*, 58−63.
(50) Chaban, V. V.; Pal, S.; Prezhdo, O. V. Laser-Induced Explosion of Nitrated Carbon Nanotubes: Nonadiabatic and Reactive Molecular Dynamics Simulations. *J. Am. Chem. Soc.* **2016**, *138*, 15927−15934.
(51) Sarkar, R.; Habib, M.; Pal, S.; Prezhdo, O. V. Tuning Charge Transfer and Recombination in Exttf/Cnt Nanohybrids by Choice of Chalcogen: A Time-Domain Density Functional Analysis. *J. Appl. Phys.* **2021**, *129*, 025501.
(52) Sarkar, R.; Kar, M.; Habib, M.; Zhou, G. Q.; Frauenheim, T.; Sarkar, P.; Pal, S.; Prezhdo, O. V. Common Defects Accelerate Charge Separation and Reduce Recombination in Cnt/Molecule Composites: Atomistic Quantum Dynamics. *J. Am. Chem. Soc.* **2021**, *143*, 6649−6656.
(53) Habib, M.; Kar, M.; Pal, S.; Sarkar, P. Role of Chalcogens in the Exciton Relaxation Dynamics of Chalcogenol-Functionalized Cdse

https://doi.org/10.1021/acs.jpcc.1c04749
J. Phys. Chem. C 2021, 125, 16620−16628

Qd: A Time-Domain Atomistic Simulation. *Chem. Mater.* **2019**, *31*, 4042−4050.
(54) Dong, S.; Pal, S.; Lian, J.; Chan, Y.; Prezhdo, O. V.; Loh, Z.-H. Sub-Picosecond Auger-Mediated Hole-Trapping Dynamics in Colloidal Cdse/Cds Core/Shell Nanoplatelets. *ACS Nano* **2016**, *10*, 9370−9378.
(55) Pal, S.; Nijjar, P.; Frauenheim, T.; Prezhdo, O. V. Atomistic Analysis of Room Temperature Quantum Coherence in Two-Dimensional Cdse Nanostructures. *Nano Lett.* **2017**, *17*, 2389−2396.
(56) Sarkar, R.; Habib, M.; Kar, M.; Pramanik, A.; Pal, S.; Sarkar, P. Structural Rigidity Accelerates Quantum Decoherence and Extends Carrier Lifetime in Porphyrin Nanoballs: A Time Domain Atomistic Simulation. *Nanoscale Adv.* **2020**, *2*, 1502−1511.
(57) Wang, Z. L.; et al. Phonon-Mediated Interlayer Charge Separation and Recombination in a Mose2/Wse2 Heterostructure. *Nano Lett.* **2021**, *21*, 2165−2173.
(58) Li, W.; She, Y. L.; Vasenko, A. S.; Prezhdo, O. V. Ab Initio Nonadiabatic Molecular Dynamics of Charge Carriers in Metal Halide Perovskites. *Nanoscale* **2021**, *13*, 10239.
(59) Zhou, G. Q.; Lu, G.; Prezhdo, O. V. Modeling Auger Processes with Nonadiabatic Molecular Dynamics. *Nano Lett.* **2021**, *21*, 756−761.
(60) Chaban, V. V.; Prezhdo, V. V.; Prezhdo, O. V. Covalent Linking Greatly Enhances Photoinduced Electron Transfer in Fullerene-Quantum Dot Nanocomposites: Time-Domain Ab Initio Study. *J. Phys. Chem. Lett.* **2013**, *4*, 1−6.
(61) Li, L. Q.; Long, R.; Prezhdo, O. V. Charge Separation and Recombination in Two-Dimensional Mos2/Ws2: Time-Domain Ab Initio Modeling. *Chem. Mater.* **2017**, *29*, 2466−2473.
(62) Long, R.; Casanova, D.; Fang, W. H.; Prezhdo, O. V. Donor Acceptor Interaction Determines the Mechanism of Photoinduced Electron Injection from Graphene Quantum Dots into TiO_2:Pi-Stacking Supersedes Covalent Bonding. *J. Am. Chem. Soc.* **2017**, *139*, 2619−2629.
(63) Stier, W.; Duncan, W. R.; Prezhdo, O. V. Thermally Assisted Sub-10 Fs Electron Transfer in Dye-Sensitized Nanocrystalline TiO_2 Solar Cells. *Adv. Mater.* **2004**, *16*, 240.
(64) Akimov, A. V.; Asahi, R.; Jinnouchi, R.; Prezhdo, O. V. What Makes the Photocatalytic Co2 Reduction on N-Doped Ta2o5 Efficient: Insights from Nonadiabatic Molecular Dynamics. *J. Am. Chem. Soc.* **2015**, *137*, 11517−11525.
(65) Zhou, Z. H.; Liu, J.; Long, R.; Li, L. G.; Guo, L. J.; Prezhdo, O. V. Control of Charge Carriers Trapping and Relaxation in Hematite by Oxygen Vacancy Charge: Ab Initio Non-Adiabatic Molecular Dynamics. *J. Am. Chem. Soc.* **2017**, *139*, 6707−6717.
(66) Sarkar, S.; Pal, S.; Sarkar, P.; Rosa, A.; Frauenheim, T. Self-Consistent-Charge Density-Functional Tight-Binding Parameters for Cd−X (X= S, Se, Te) Compounds and Their Interaction with H, O, C, and N. *J. Chem. Theory Comput.* **2011**, *7*, 2262−2276.
(67) Saha, S.; Pal, S.; Sarkar, P.; Rosa, A.; Frauenheim, T. A Complete Set of Self-Consistent Charge Density-Functional Tight-Binding Parametrization of Zinc Chalcogenides (Znx; X= O, S, Se, and Te). *J. Comput. Chem.* **2012**, *33*, 1165−1178.
(68) Bussi, G.; Donadio, D.; Parrinello, M. Canonical Sampling through Velocity Rescaling. *J. Chem. Phys.* **2007**, *126*, 014101.
(69) Grubmüller, H.; Heller, H.; Windemuth, A.; Schulten, K. Generalized Verlet Algorithm for Efficient Molecular Dynamics Simulations with Long-Range Interactions. *Mol. Simul.* **1991**, *6*, 121−142.
(70) Nelson, T. R.; Prezhdo, O. V. Extremely Long Nonradiative Relaxation of Photoexcited Graphane Is Greatly Accelerated by Oxidation: Time-Domain Ab Initio Study. *J. Am. Chem. Soc.* **2013**, *135*, 3702−3710.
(71) Rush, T. S.; Kozlowski, P. M.; Piffat, C. A.; Kumble, R.; Zgierski, M. Z.; Spiro, T. G. Computational Modeling of Metalloporphyrin Structure and Vibrational Spectra: Porphyrin Ruffling in Nitpp. *J. Phys. Chem. B* **2000**, *104*, 5020−5034.
(72) Mukamel, S. *Principles of Nonlinear Optical Spectroscopy*; Oxford University Press: New York, 1995; Vol. *6*.
(73) Kilina, S. V.; Neukirch, A. J.; Habenicht, B. F.; Kilin, D. S.; Prezhdo, O. V. Quantum Zeno Effect Rationalizes the Phonon Bottleneck in Semiconductor Quantum Dots. *Phys. Rev. Lett.* **2013**, *110*, 180404.
(74) Itano, W. M.; Heinzen, D. J.; Bollinger, J.; Wineland, D. Quantum Zeno Effect. *Phys. Rev. A: At., Mol., Opt. Phys.* **1990**, *41*, 2295.
(75) Li, J.; Ambroise, A.; Yang, S. I.; Diers, J. R.; Seth, J.; Wack, C. R.; Bocian, D. F.; Holten, D.; Lindsey, J. S. Template-Directed Synthesis, Excited-State Photodynamics, and Electronic Communication in a Hexameric Wheel of Porphyrins. *J. Am. Chem. Soc.* **1999**, *121*, 8927−8940.
(76) Wagner, R. W.; Seth, J.; Yang, S. I.; Kim, D.; Bocian, D. F.; Holten, D.; Lindsey, J. S. Synthesis and Excited-State Photodynamics of a Molecular Square Containing Four Mutually Coplanar Porphyrins. *J. Org. Chem.* **1998**, *63*, 5042−5049.
(77) Philippa, B.; Stolterfoht, M.; White, R. D.; Velusamy, M.; Burn, P. L.; Meredith, P.; Pivrikas, A. Molecular Weight Dependent Bimolecular Recombination in Organic Solar Cells. *J. Chem. Phys.* **2014**, *141*, 054903.
(78) Dixon, A. G.; Visvanathan, R.; Clark, N. A.; Stingelin, N.; Kopidakis, N.; Shaheen, S. E. Molecular Weight Dependence of Carrier Mobility and Recombination Rate in Neat P3ht Films. *J. Polym. Sci., Part B: Polym. Phys.* **2018**, *56*, 31−35.

https://doi.org/10.1021/acs.jpcc.1c04749
J. Phys. Chem. C 2021, 125, 16620−16628